QUEST
BORN TO ENGINEER

uniform crystal temperature sensor accuracy under transient conditions

This paper investigates the accuracy of Uniform Crystal Temperature Sensors (UCTS) under transient conditions and describes a methodology for addressing sources of systematic error based on the findings.

Jason DeVoe
QuEst Global Services-NA, Inc.
Phoenix, AZ, USA

Stephen Odom
QuEST Global Services-NA, Inc.
Phoenix, AZ, USA

Lev Ginzbursky
LG Tech-Link, LLC
Chandler, AZ, USA

contents

Abstract

This paper investigates the accuracy of Uniform Crystal Temperature Sensors (UCTS) under transient conditions and describes a methodology for addressing sources of systematic error based on the findings. The study applies to the important task of thermal mapping of critical turbine parts during the engine development phase, for which UCTS is particularly well suited [1, 2, 3, 4]. A previous study focused on UCTS in steady state regimes and provided recommendations for optimizing the technique [5]. However, a substantial reduction in engine development costs may be achieved by being able to combine, for instance cyclic endurance tests with thermal mapping assuming that neither task will jeopardize the other.

The basic trends and magnitude of measurement errors were assessed as a function of factors such as UCTS installation configuration, thermo-physical properties of the installation materials and cycle characteristics. The authors used Finite Element Analysis to simulate transient heat transfer through a thin wall with an embedded UCTS. Stress calculations performed for the case of densely packed multi-UCTS installation on turbine blades showed no detrimental influence of standard micro-cavities on blade structural characteristics. These results were confirmed by a number of successful endurance tests, proving its compatibility with the task of thermography. Attention was focused on the cyclic test influence on the accuracy of thermal mapping. Single and multiple cycle test configurations have been considered

After completion of a computational matrix, the characteristic results of interest are presented in the form of plots and diagrams to support the technical discussion. Recommendations drawn from this research will help analytical designers, test and instrumentation engineers to plan and execute dual task transient tests with a high accuracy of thermal mapping result interpretation.

Introduction

Substantial advances in computational heat transfer and fluid dynamics have significantly improved the quality of analytical predictions [6, 7]. Sophisticated experiments performed in the lab environment provide a basis for more accurate algorithm development in the models, but still cannot be fully generalized to the real engine environment [8]. Despite the improvements in these capabilities, uncertainty exists and the need to verify the results of engineering thermal analysis remains critical.

Currently, the turbo machinery industry utilizes a range of available metal temperature measurement techniques. Selection of one tool over another is driven in large part by the objectives of a given task. Using the domain of application as a general guide, a systematic overview of available methods may be organized with respect to four general functions:

- Engine performance optimization in field conditions with a sensor providing a flow of information to the onboard computer (FADEC, etc.)
- Engine condition monitoring during field operations, where metal temperature measurements are used to improve engine maintenance and diagnostic techniques
- Cold/warm laboratory rigs and blow down wind tunnel testing to obtain validation data for the development of new algorithms to be used in heat transfer analytical modeling codes
- Thermal mapping of critical engine parts during the engine development cycle to validate analytical predictions

The first two activities require in-situ measurement and, real-time communication. Engine performance optimization and engine condition monitoring applications also dictate a need for robustness capable of surviving real engine conditions, but do not require accuracy in absolute temperature measurement. The objective of these activities is to monitor the trends with accuracy, and not necessarily to measure the temperature value itself. In contrast, the task of lab validation, places a premium on accuracy and sensors must be capable of quantitative characterization of the individual temperatures as well as their distribution in typical turbine parts. This is possible using very fragile elements, but they are limited to use in lab conditions.

For the fourth domain, the experimental technique used in thermal mapping must demonstrate high standards of accuracy to be used effectively for analytical prediction verification but be robust enough for working in real engine conditions.

Uniform Crystal Temperature Sensor (UCTS) technology is not appropriate to the first three functions. However, it is particularly well suited for the fourth. It is robust, highly accurate in individual temperature measurements, microscopic in size, and does not require wire connectors. These characteristics make it highly compatible with the harsh engine environment and the task of analytical design code verification.

Thermocouples, thermal paints and pyrometry are also used in this domain. Each method is well documented and the influences of uncertainties that are present in the complex reality of the engine flow path (factors such as radiation, absorption, flow interference, etc.) have been well studied. Concise surveys of these methods are available in a number of publications [9, 10, 11].

The principle of UCTS application requires embedding the sensor into the metal wall of the parts, which isolates it from the complexities and harshness of the external gas flow environment. Made of SiC, which is one of the most temperature resistant materials, the UCTS is fixed in place using a temperature resistant and highly adhesive cement. Its principle of operation employs the simplest form of heat transfer, which is thermal conduction.

The combination of UCTS characteristics is attractive to engine developers, especially when applied to rotating and hard to access parts. In spite of the fact that the UCTS method is less vulnerable to systematic error, it is important to investigate the ways of reducing these potential errors or compensating for them. The first step in this direction was made for steady state conditions [4]. In this paper, the authors are researching the trends for accuracy in typical transient conditions. Specifics of UCTS installation and application will require careful ANSYS modeling for three major installation configurations and variations in thermo-physical properties of the installation material. Results of this study will help practicing engineers apply the UCTS technique with confidence and in combination with other tests.

Numerical Approach and Boundary Conditions

The computational matrix was constructed to embrace variations in:

- Installation configuration
- Thermo-cement conductivity
- Cycle temperature overshoot

The single cycle definition, shown in Figure 1, was derived from [12]. A sequence of five identical cycles was investigated as a separate case study.

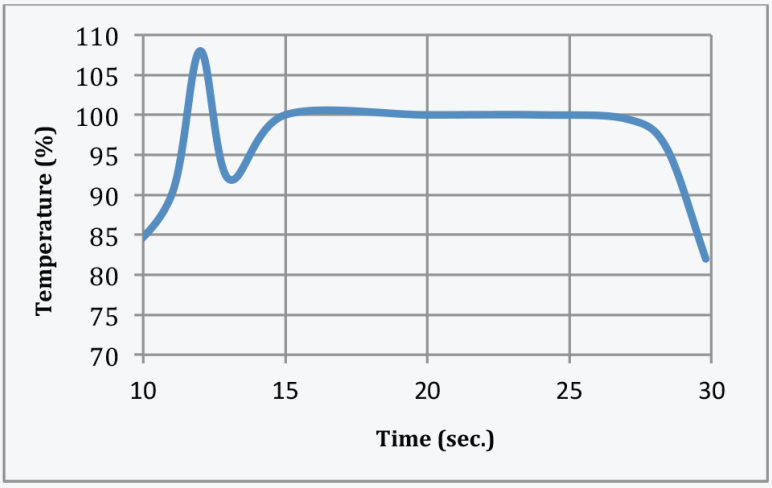

Figure 1. Single Cycle Definition

Data Reduction and Analysis

The following steps must be implemented to obtain the necessary computational results:

1. Based on the ANSYS solution, identify $\mathbf{T_{ucts\ max}}$
2. Plot ($\mathbf{T_{ucts}}$ / $\mathbf{T_{ucts\ max}}$ **vs. Time**) to use as the time diagram
3. Use a Calibration Nomogram to obtain crystal lattice characteristics (**DBA**, also known as Double Bragg Angle), which would be measured by an X-ray Diffractometer if the sensor would be exposed to $\mathbf{T_{ucts\ max}}$ for the period of time which is equivalent to the ($\mathbf{T_{ucts}}$ / $\mathbf{T_{ucts\ max}}$ **vs. Time**) cycle
4. Assume two scenarios: a) an engine test conducted with an Exit Gas Temperature (EGT) thermocouple that is used to produce the time diagram, and b) an engine test with a reference thermocouple embedded into the metal wall
5. Using the Calibration Nomogram, find for **DBA** obtained in step 3 and the time diagrams developed in step 4 for the values of maximum metal temperature corresponding to both scenarios: $\mathbf{T_{egt\ max}}$ and $\mathbf{T_{m.g.s.\ max}}$
6. Compare data reduction results with $T_{m.max}$ (metal temperature at the undisturbed sensor-depth location) to define the measurement error using:

$$\theta = \frac{T_{m.max} - T_{calc}}{T_{m.max}} \times 100\% \qquad (1)$$

Where T_{calc} can be either T_{egt} or $T_{m.g.s.}$ based.

Figure 2 illustrates assumed locations for temperatures T_{egt}, $T_{m.g.s.}$, T_{ucts} and $T_{m.}$.

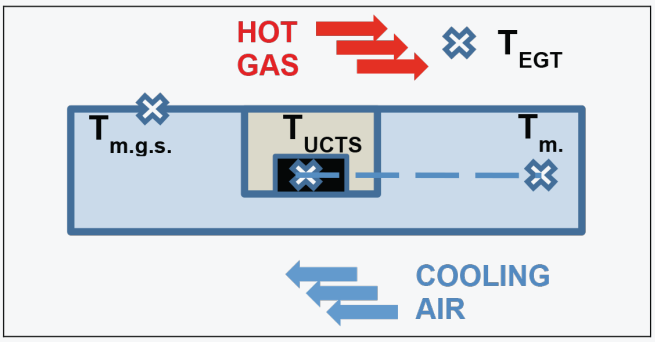

Figure 2. Notation For Data Reduction Algorithm

Geometrical Models

The UCTS has a rectangular prism shape, with the dimensions of 0.20 × 0.20 × 0.38 mm. It is installed into a thin metal wall. The wall thickness is 1.0 mm and the size and material of the wall has been chosen to represent the critical elements of turbine engine parts such as a combustor liner, nozzle vane, and rotor blade. The three UCTS installation configurations used in this wall are pictured in Figure 3.

In all cases, the installation cavity has a diameter of 0.7 mm and a depth of 0.625 mm. In all three configurations, the sensor is positioned at the bottom of the cavity and is secured in place by thermo-cement. Additionally, an analysis of UCTS positioning within the cavity was performed for configuration A. This analysis contrasts the difference between installing the UCTS horizontally and vertically. In configuration B, as an additional measure of security, a 0.05 mm thick metal shim with a diameter of 1.5 mm is spot-welded over the top of the cavity. Configuration C includes a layer of thermo-barrier coating (TBC) applied over the top of the metal wall. The thickness of the TBC is 0.2 mm.

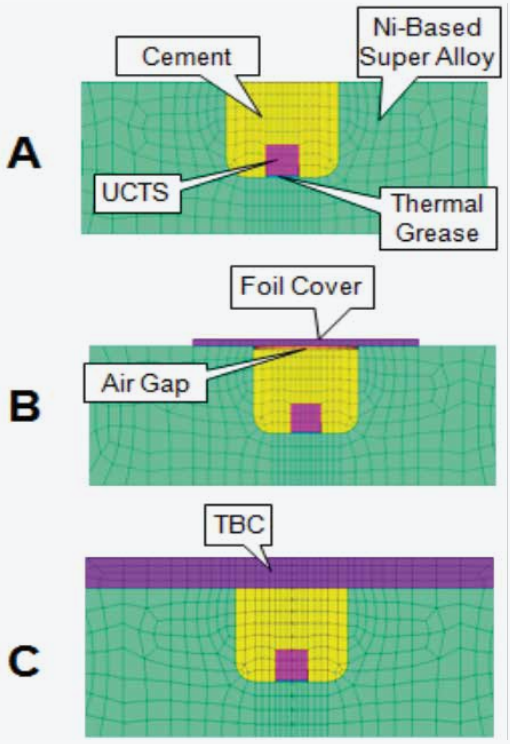

Figure 3. Installation Configurations

Material Properties

Thermo-physical characteristics for all elements of the wall sensor assembly filler system are listed in Table 1.

Table 1. Thermo-physical Characteristics of The Wall Sensor Assembly Filler System

Elements of Sensor Installation Assembly	K-Thermal Conductivity Coefficient [W/ m- °C]	Comments
UCTS sensor (Irradiated SiC)	20	
Thin wall (Ni-based super alloy)	26	
TBC coating	1	Zirconia
Resbond 919	0.6	Thermo-cement
Resbond 906	6.0	Thermo-cement

The design point operating conditions were taken from a NASA EEE Report [13]. A Summary of this information is provided in Table 2.

Table 2. Reference Parameters

Reference Parameter	Value
T_{gas}	1739.4 °C
$T_{c.air}$	696.1 °C
htc_{gas}	5252.7 W/m^2 °C
$htc_{c.air}$	7183.4 W/m^2 °C
Cp_{metal}	0.098 cal/g °C
Cp_{sensor}	0.180 cal/g °C
Cp_{cement}	0.340 cal/g °C
ρ_{metal}	8.44 g/cm^3
ρ_{sensor}	3.1 g/cm^3
ρ_{cement}	1.66 g/cm^3

To ratio the boundary conditions during the transient cycle, the variations in thermal properties had been included at each time point. The scalers were derived on the basis of correlations taken from [14] and typical engine characteristics presented in [12]. This scalers formula is described by the following:

$$\frac{htc@power}{htc@baseline\ power} \sim \frac{(m \times Re_x^{0.8} \times Pr^{0.33})@\ power}{(m \times Re_x^{0.8} \times Pr^{0.33})@\ baseline\ power} \quad (2)$$

During the test, the UCTS accumulates changes in its crystal lattice structure due to the temperature level and time of exposure. In general terms, this could be expressed as follows:

$$DBA = A + B \times T + C \times \log(t) \quad (3)$$

- DBA (Double Bragg Angle, which is the lattice characteristic measured by an X-ray Diffractometer after the test)
- A, B, C are constants
- T is temperature (degrees Celsius)
- t is time (minutes).

A series of these curves obtained experimentally during the calibration process, and put together will form the calibration nomogram, shown in Figure 4.

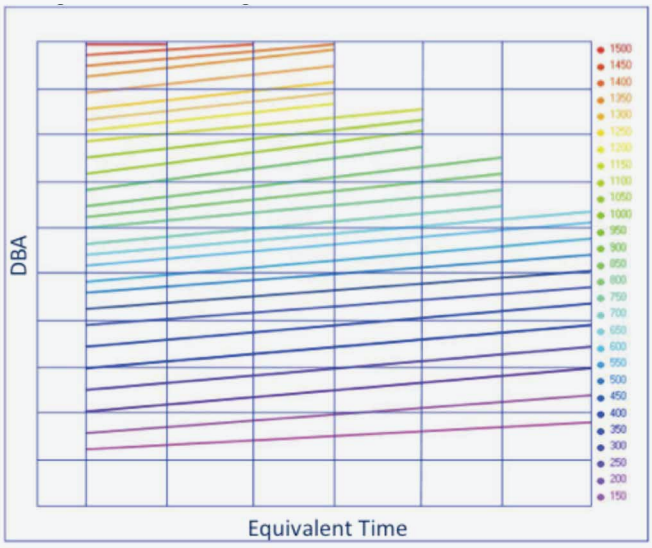

Figure 4. Calibration Nomogram

Exit Gas Temperature (EGT) thermocouples are often used to generate a time diagram record as shown in Figure 5.

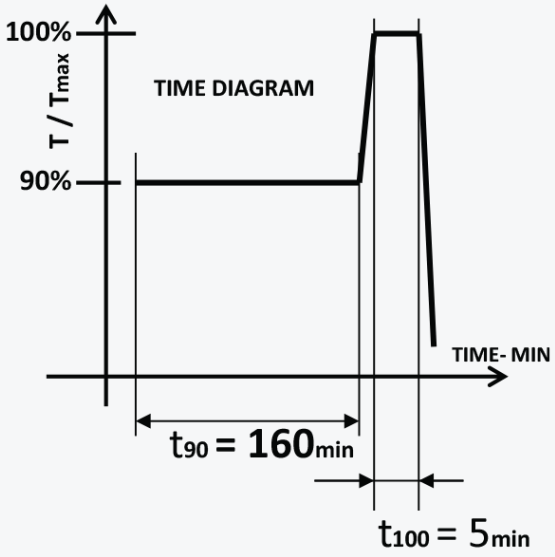

Figure 5. Time Diagram

The assumption made here is that the character of the temperature level variation is identical for both the reference thermocouple and the temperature at the location of this sensor. Apply equation (3) to the two sets of variables. In one we will use the real time and temperature, and in the other we will use T (max) and t equivalent. To satisfy the principle of equivalency, the values of DBA, in both cases, must be equal to each other. Mathematically, this will be expressed as the following:

$$A + B \times T_{max} + C \times \log(t_{eqv}) = A + B \times T + C \times \log(t) \quad (4)$$

After performing a simple algebraic transformation, the expression for the time equivalency coefficient can be derived:

$$N_{eqv} = \frac{t}{t_{eqv}} = 10^{\frac{B \times T_{max} \times (1-\alpha)}{C}} \quad (5)$$

In the above equation (5) α represents the normalized temperature $T/T_{max.}$

Figure 6 gives a graphical representation of this equation for the set of constants, which are characteristic for one of the calibration nomograms.

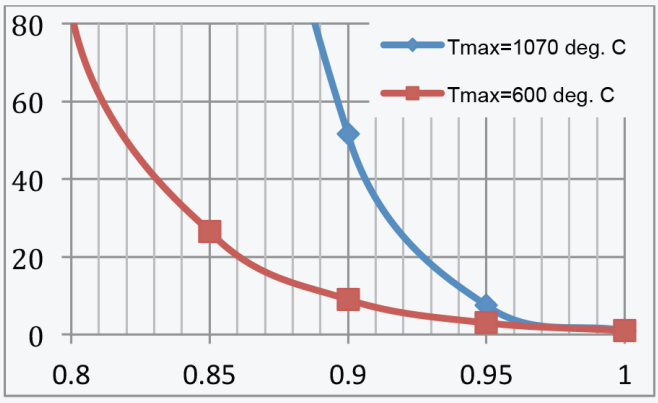

Figure 6. N_{eqv} VS.T/T_{max}

In this example, one can see that for the T/T_{max} = 0.9 (Figure 6), based on the T_{max} = 1070 °C curve, 160 minutes spent at this regime (Figure 5) will be considered equivalent to the effect of 1/50th of that time spent at T_{max} in terms of the crystal lattice modification. At the end, the value of teqv for every time diagram should be expressed as:

$$t_{eqv} = t_{max} + \sum(t_i / N_{eqv}) \quad (6)$$

Now, with the DBA value measured by a lab X-ray diffractometer and teqv calculated according to (6), the calibration nomogram (Figure 4) is used to find the corresponding maximum metal temperature experienced by UCTS (T_{max}) during an engine test procedure.

Results and Discussion

Numerical experimentation conducted using the previously described methodology produced the data necessary for analysis. Figure 7 demonstrates an example of the typical output. In this particular case, variation in temperature vs. time is superimposed on the same plot to illustrate their relationship in the transient process. The case in study is Installation Configuration A-Overshoot 8%, high conductivity cement. The general characteristics of the cycle for all four temperatures are compatible with intuitive expectations. Temperatures during the cycle, behave in accordance with the single cycle definition assumptions. The values of the temperature decrease from T_{egt} to the temperature on the metal wall surface from the gas side to the level of sensor center of gravity (CG) location.

This particular graph shows them practically superimposed on each other, and illustrates that there is good agreement during all of the cycle between the temperature of the metal wall in the undisturbed region, and the temperature of the sensor. Similar sets of information were obtained for all cases constituting the computation matrix.

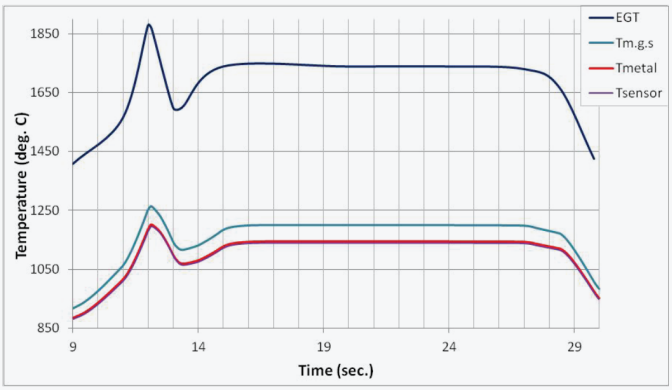

Figure 7. Configuration A, Overshoot 8%, High Conductivity Cement

In addition to single cycle analysis, a sequence of five identical cycles had been analyzed. Figures 8 and 9 how the results of this study for cases with low and high conductivity cements, for the same installation configuration (Configuration A), and overshoot (8%). It should be noted that the multicyclic runs did not change the parameters of any of the individual cycles.

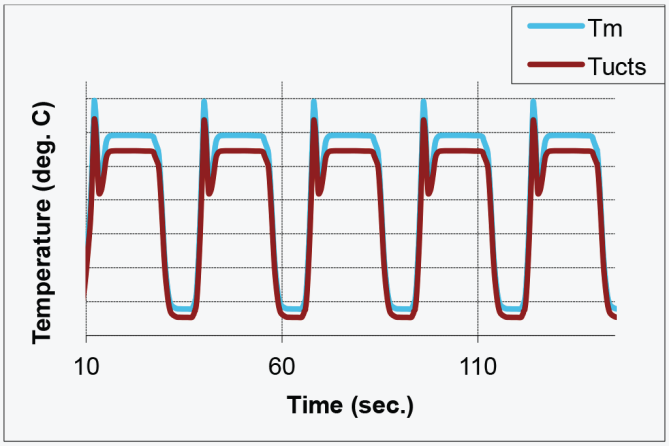

Figure 8. Cycle Analysis For Low Conductivity Cement

Positioning of the metal temperature (T_m) and sensor temperature (T_{ucts}) on the same chart illustrates the influence of cement conductivity on the difference between the true temperature of the metal wall and the temperature measured by the sensor.

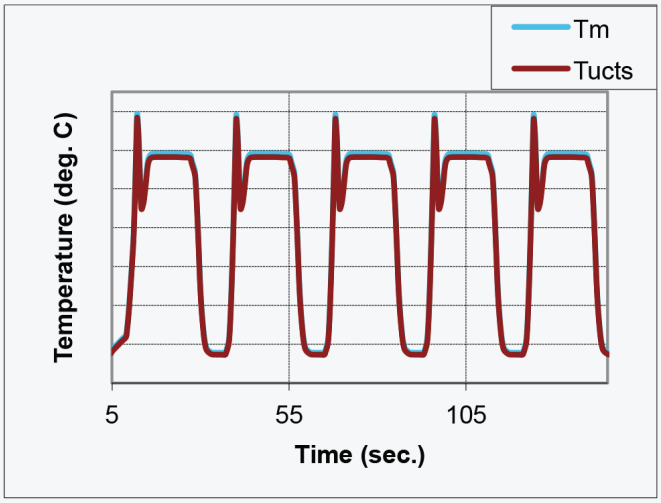

Figure 9. Cycle Analysis For High Conductivity Cement

To understand the phenomenon in more detail, it is useful to take a look at the temperature contour plots in Figures 10, 11, and 12. All are plotted for the maximum cycle point for each installation configurations. The visualizations clearly depict the temperature field distortions that exist in the vicinity of the installation packages.

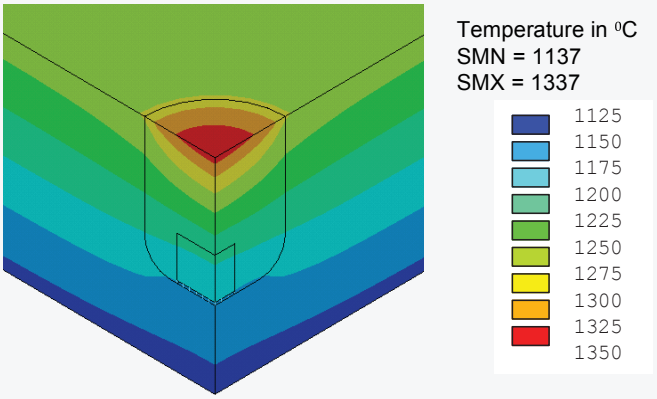

Figure 10. Configuration A, 8% Overshoot, High Conductivity Cement

Configurations A and B are quite similar, in spite of the metallic shim cap spot welded locally over the top of the installation cavity in Configuration B.

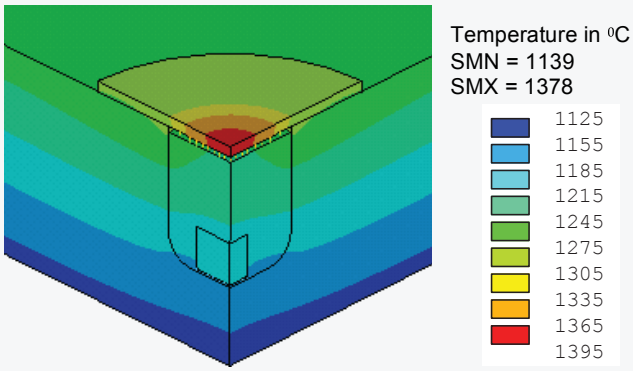

Figure 11. Configuration B, 8% Overshoot, High Conductivity Cement

However, Configuration C presents a special case, because a layer of TBC is applied on the gas side surface of the wall. Forunately, all of these nuances are easily modeled by Finite Element Analysis, and could be taken into account in combination with specific boundary conditions to produce a reliable quantative result.

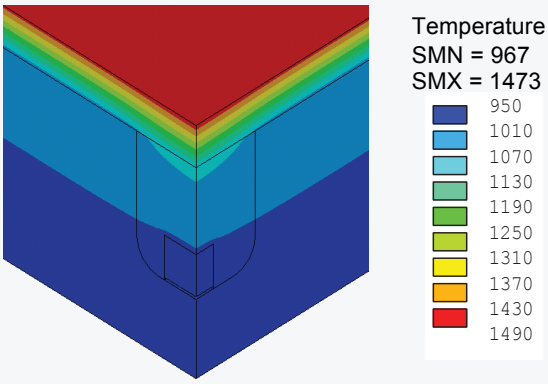

Figure 12. Configuration C, 8% Overshoot, High Conductivity Cement

In Figure 13, Configuration A, 8% overshoot is used to demonstrate a typical temperature cycle. This comparison shows that there is an insignificant cycle phase shift. Also noticeable is significant peak attenuation. Almost all attenuation takes place between the hot gas free stream temperature (EGT type thermocouple measurement) and the temperature measured at the metal wall thermocouple location ($T_{m.g.s}$).

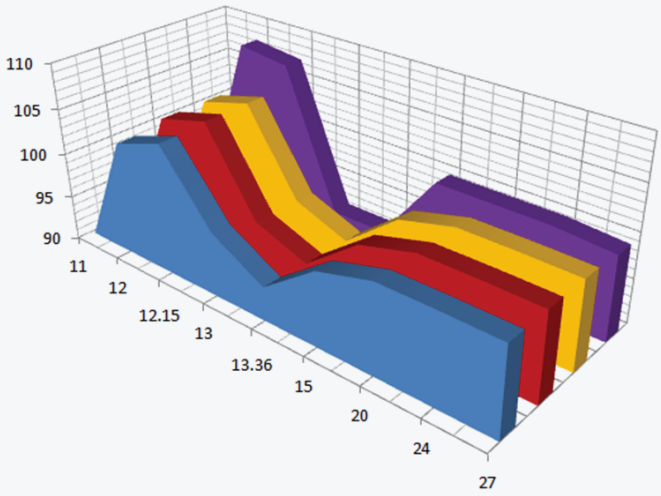

	11	12	12.15	13	13.36	15	20	24	27
Sensor - Low k	88.8	102.6	104.6	97.2	93.8	98.3	100	100	99.9
Sensor - High k	88.8	103.3	104.9	95.8	93.6	98.3	100	100	99.9
Metal Temp	88.8	103.3	104.9	95.8	93.5	98.4	100	100	99.9
Hot Gas (EGT)	90	108	107.3	92	92	100	100	100	99.5

Figure 13. Temperature Cycle Overshoot Attenuation ($T/_{tnom}$*100% Vs. Time)

For this specific installation configuration geometry, material properties and assumed boundary conditions, the model shows that the cyclic temperature peak for the 8% Gas Temperature overshoot was reduced from 8% to 4.6%.

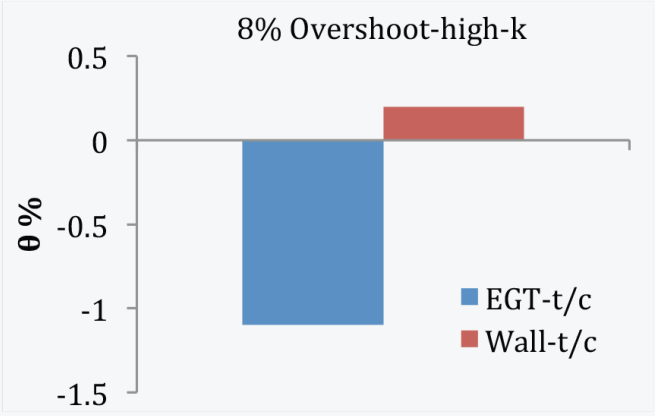

Figure 14. Measurement Error Comparison - Configuration A

The danger of this phenomenon, as described in the data reduction procedure, is that the accuracy of measurement depends on how well the physics of heat transfer at the sensor location is represented by the reference time diagram. Using an EGT thermocouple as a reference in the case of aggressive cycling will inevitably bring measurement error even for the high thermo-cement conductivity cases. Figures 14, 15, and 16 illustrate this point showing that this pattern exists for all three installation configurations.

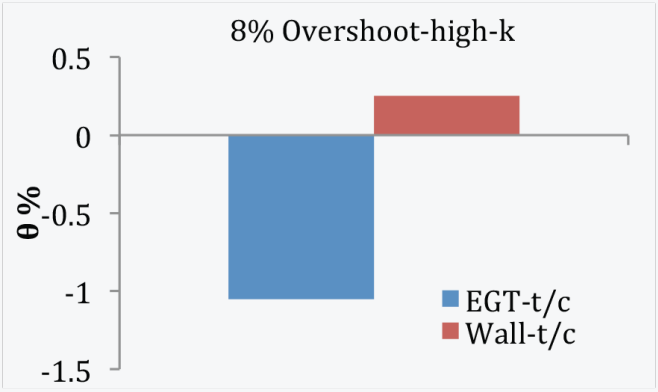

Figure 15. Measurement Error Comparison - Configuration B

The error assessment was made using equation (1).

$$\theta = \frac{T_{m.max} - T_{calc}}{T_{m.max}} \times 100\% \qquad (1)$$

In this case $T_{m.max}$ is the ANSYS calculated value of the maximum temperature of the metal wall in the undisturbed sensor installation area located at the same depth from the hot gas surface as the Center of Gravity (CG) of the sensor installed in this wall (assumed as true temperature). Tcalc is the metal temperature calculated using the UCTS data reduction procedure based on EGT time diagram or the wall-embedded thermocouple diagram. To improve the quality of low temperature measurement, it is necessary to make corrections to the EGT produced diagram or to find a location for the installation of the reference thermocouple that will better represent the temperature cycle experienced by the sensor. Analytical modeling could be a very useful tool for this correction procedure.

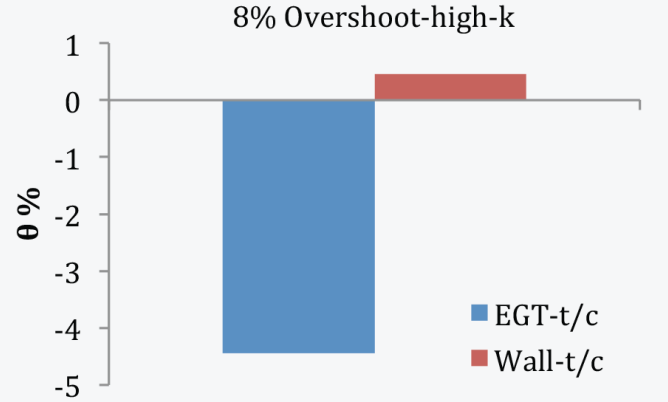

Figure 16. Measurement Error Comparison - Configuration C

The results discussed in this paper are representative of basic trends and exemplify the possible sources of systematic error. The recommendations describe a methodology that can be applied to come up with appropriate corrections based on the geometry, boundary layer conditions and other factors unique to the design in question. The most important thing is to find the sources of error and determine the correction factor to apply. It is up to the experimenter to find, for example, the heat transfer inertia, calculating it using numerical experiments or obtaining it from physical investigations. The UCTS technique uses x-ray diffractometry to measure real changes in the crystal, which are dependent on physical conditions during the full length of the test. If the physical location is represented with error, as seen in the EGT case, it will translate into temperature error. The goal should be to reduce or eliminate such discrepancy.

It can be assumed that this kind of phenomenon does not exist for the non-cyclic or non-aggressive cyclic situations. The authors intentionally took under analysis the most difficult case to provide guidance that will enable a broader use of UCTS beyond dedicated testing.

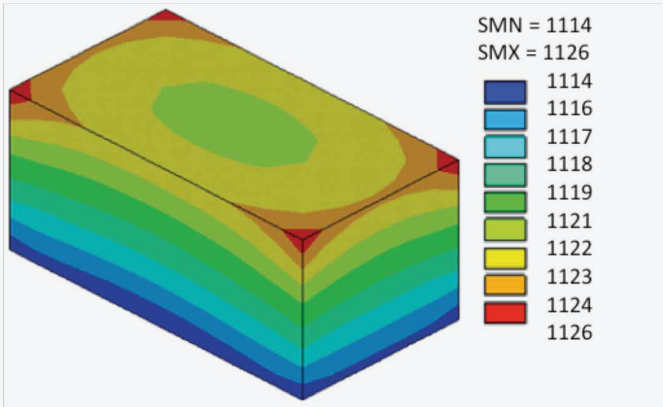

Figure 17. Ucts In Horizontal Position (0.2 X 0.38 Mm Face Down)

To improve understanding of the effects of UCTS installation positioning a separate investigation was performed to analyze the differences between a UCTS positioned on the bottom of the cavity with the 0.2 x 0.38 mm face down, horizontal position (Figure 17), versus a UCTS installed with the 0.2 x 0.2 mm face down, vertical position (Figure 18). It was assumed in all cases that the UCTS would be interrogated by an X-Ray Diffractometer from any of the 0.2 x 0.2 mm sides.

The presented contour plots show no temperature gradients in the horizontal direction. In this case the results of X-Ray diffractometry and the subsequent result of data reduction would be assigned to the CG of the UCTS. This is the recommended sensor position for metal temperature measurement.

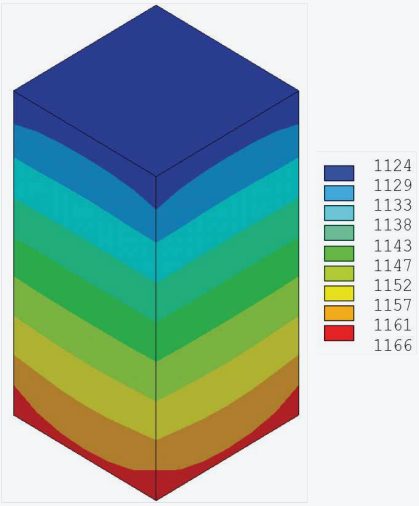

Figure 18. Ucts In Vertical Position (0.2 X 0.2 Mm Face Down)

The result of analysis for the vertical position of the UCTS showed the potential to measure temperature gradients in the vertical direction. In this case, because of the UCTS size and existing heat flux through the wall, the gradients were not large enough to claim that an accurate measurement of the temperature gradient and heat flux could be obtained. It might be suggested that physical and numerical experimentation should be continued with several UCTS stacked on top of each other, where the size of the cavity and the wall will allow it to realize the full scale potential of this unique sensor.

Conclusions and Recommendations

The single cycle configuration chosen for this study wasintentionally designed to represent the worst-case scenario. It was used to investigate the possible systematic errors in maximum temperature measurement by UCTS method in transient conditions. It allowed the authors to study trends in developing errors, and to understand potential means by which to reduce or eliminate them all together.

On the basis of the performed study, it is concluded that the accuracy of temperature measurement in the thin wall during transient conditions could be greatly improved if the following recommendations are applied:

- The highest conductivity thermal cement should be used for the installation package
- A switch from Resbond 919 to Resbond 906 will be satisfactory in most cases

It is also very important to recognize that the use of a time diagram based on an EGT type thermocouple in aggressive cycles could be the source of additional error due to the fact that it does not accurately represent the physics of the heat transfer situation in the metal wall. An analytical study for each particular case with its own set of boundary and geometrical conditions could provide valuable information on the expected rate of attenuation and allow the time diagram to be corrected accordingly. Another way to deal with this problem would be to choose as a reference the thermocouple attached to the local metal structure. The time diagram produced by this thermocouple should be more reflective of the real characteristics of the temperature cycle. It is worthwhile to note that in this study the authors assumed no thermal inertia for the EGT thermocouples.

Finally, it is important to emphasize the necessity of close cooperation between analytical engineers and instrumentation specialists to closely monitor the physics of the process of the temperature measurement to produce the highest accuracy of measurement possible in the harsh engine environment.

Acknowledgments

The authors would like to thank Dr. Y. Shekhtman for his guidance and technical support in developing the UCTS Data Reduction methodology.

Nomenclature

CG	Center of gravity
Cp	Specific heat capacity
Cp_{cement}	Specific heat capacity of cement
Cp_{metal}	Specific heat capacity of base metal
Cp_{sensor}	Specific heat capacity of sensor material
DBA	Double Bragg Angle
EGT	Exit Gas Temperature, °C
FADEC	Full Authority Digital Energy Control
htc	Heat transfer coefficient, W/m2- °C
$htc_{c.air}$	Cooling air heat transfer coefficient
htc_{gas}	Gas heat transfer coefficient
K	Conductivity coefficient, W/m- °C
m	Constant in scalers equation
N_{eqv}	Time equivalency coefficient
Overshoot	T_{max} / T_{nom}
ρ	Density
ρ_{cement}	Cement density
ρ_{metal}	Metal density
ρ_{sensor}	Sensor density
Pr	Prandtl number
Re	Reynolds number
SiC	Silicon Carbide
t/c	Thermocouple
t_{eqv}	Equivalent time
$T_{c.air}$	Temperature of cooling air, °C
T_{calc}	Calculated max temperature based on time diagram from EGT or the embedded reference thermocouple, °C
T_{egt}	Exit gas temperature, °C
$T_{egt\ max}$	Maximum exit gas temperature, °C
T_{gas}	Gas temperature, °C
T_{m}	Temperature at the undisturbed sensor depth location, °C
$T_{m.max}$	Maximum temperature at the undisturbed sensor depth location, °C
$T_{m.g.s.\ max}$	Temperature of the metal wall on gas side, measured using the embedded reference thermocouple, °C
T_{nom}	Nominal (target 100%) temperature, °C
T_{ucts}	Temperature at the CG location of the UCTS, °C
$T_{ucts\ max}$	Maximum temperature at the CG location of the UCTS, °C
TBC	Thermo Barrier Coating
UCTS	Uniform Crystal Temperature Sensor
α	Normalized temperature, T / T_{max}
θ	Error

Subscripts

c.air	Cooling air
egt max	Exit gas temperature maximum
m.max	Metal maximum at the undisturbed sensordepth location
m.g.s. max	Metal wall gas side maximum
nom	Nominal, Target100%

References

1. Ginzbursky, L. 2010. “UCTS: How It Works”. http://www.lgtechlink.com.
2. Nikolaenko, V.A., Morosov, V.A., Kasianov, N.I. 1976. “Crystal Maximum Temperature Measurer for Special Applications”. Rev. Int. Htes Temp. et Refract, 13, pp. 17-20.
3. Shukin, S., Annerfeldt, Mats., Bjorkman, Mats. 2008. “Siemens SGT-800 Industrial Gas Turbine Enhanced to 47MW. Design Modifications and Operation Experience”. ASME Turbo Expo 2008: Power for Land, Sea, and Air, GT2008-5008, 7, pp. 65-70.

4. Malak, M., Liu, J., Zurmehly, E., Rosales, J.L., 2011. "Turbine Shroud Durability Analysis Using Time Unsteady CFD and Si-C Testing". Proceeding of ISABE 2011, ISABE-2011-1706.

5. Devoe, J., Ginzbursky, L., Romanov, D. 2011. "Optimization of Temperature Measurement Technique Used in High Heat Flux Environment". Proceedings of ASME Turbo Expo 2011 GT2011-45269.

6. Clark, J.P., Downs, J., Fan, G., Ho Ni, R., Humber, W., Koch, P.J. 2011. "Conjugate Heat transfer Analysis of a Film-Cooled Turbine Vane". Proceedings of ASME Turbo Expo 2011 GT2011-45920.

7. Luo, J., Razinsky, E., Moon, H. 2011. "3D RANS Prediction of Gas-Side Heat Transfer Coefficients on Turbine Blade and Endwalls". Proceedings of ASME Turbo Expo 2011 GT2011-46723.

8. Kahveci, H., Haldeman, C., Dunn, M. 2011. "Heat Transfer for the Film-Cooled Vane of a 1-1/2 Stage High- Pressure Transonic Turbine – Part II – Effect of Cooling Variation on the Vane Airfoil and Inner Endwall". Proceedings of ASME Turbo Expo 2011 GT2011-46573.

9. Li, H., Wang, G., Nirmalan, N., Dasgupta, S. 2011. "Passive Absorption/Emission Spectroscopy for Gas Temperature Measurements in Gas Turbine Engines". 2011. Proceedings of ASME Turbo Expo 2011 GT2011- 45152.

10. Rabhiou, A., Feist, J., Kempf, A., Skinner, S., Heyes, A. 2011. "Phosphorescent Thermal History Sensors". Sensors and Actuators A.

11. Childs, P. 2001. Practical Temperature Measurement. Butterworth-Heinemann, Oxford, UK.

12. Heiser, W.H., Mattingly, J.D., Pratt, D.T. 2002. AAA Education Series: Aircraft Engine Design Second Edition. American Institute of Aeronautics and Astronautics, Inc. Reston, VA. Editor J.S. Przemieniecki.

13. Halila, E.E., Lenahan, D.T., and Thomas T.T. June 1982. "High Pressure Turbine Test Hardware Detailed Design Report". NASA-CR-167955

14. Bergman, T.L., Dewitt, D.P., Incropera, F.P., Lavine, A.S. 2007. Fundamentals of Heat and Mass Transfer Sixth Edition. John Wiley & Sons. Danvers, MA

About QuEST Global

QuEST Global is a focused global engineering solutions provider with a proven track record of over 17 years serving the product development & production engineering needs of high technology companies. A pioneer in global engineering services, QuEST is a trusted, strategic and long term partner for many Fortune 500 companies in the Aero Engines, Aerospace & Defence, Transportation, Oil & Gas, Power, Healthcare and other high tech industries. The company offers mechanical, electrical, electronics, embedded, engineering software, engineering analytics, manufacturing engineering and supply chain transformative solutions across the complete engineering lifecycle.

QuEST partners with customers to continuously create value through customer-centric culture, continuous improvement mind-set, as well as domain specific engineering capability. Through its local-global model, QuEST provides maximum value engineering interactions locally, along with high quality deliveries at optimal cost from global locations. The company comprises of more than 7,000 passionate engineers of nine different nationalities intent on making a positive impact to the business of world class customers, transforming the way they do engineering.

QUEST

BORN TO ENGINEER

http://quest-global.com